Article

Immunity

CXCR3 Chemokine Receptor Enables Local CD8$^+$ T Cell Migration for the Destruction of Virus-Infected Cells

Highlights

- CXCR3 ligands are upregulated in VV-infected skin
- *Cxcr3*$^{-/-}$ mice have normal T cell numbers in infected skin but enhanced infection
- *Cxcr3*$^{-/-}$ T cells are defective in locating virus-infected cells for killing in situ
- Transfer of wild-type CD8$^+$ T cells restores viral control in *Cxcr3*$^{-/-}$ animals

Authors

Heather D. Hickman, Glennys V. Reynoso, ..., Jack R. Bennink, Jonathan W. Yewdell

Correspondence

hhickman@mail.nih.gov

In Brief

The factors that guide antiviral cytotoxic T cells migrating within tissues to their virus-infected targets are unclear. Hickman and colleagues show that CXCR3 expression on CD8$^+$ T cells enhances their ability to locate infected cells in the skin and thus maximizes viral clearance.

Hickman et al., 2015, Immunity *42*, 524–537
March 17, 2015
http://dx.doi.org/10.1016/j.immuni.2015.02.009

CellPress

CellPress

Immunity
Article

CXCR3 Chemokine Receptor Enables Local CD8$^+$ T Cell Migration for the Destruction of Virus-Infected Cells

Heather D. Hickman,[1,*] Glennys V. Reynoso,[1] Barbara F. Ngudiankama,[1] Stephanie S. Cush,[1] James Gibbs,[1] Jack R. Bennink,[1] and Jonathan W. Yewdell[1]

[1]Cell Biology and Viral Immunology Sections, Laboratory of Viral Diseases, National Institutes of Allergy and Infectious Diseases, NIH, Bethesda, MD 20892, USA

*Correspondence: hhickman@mail.nih.gov

http://dx.doi.org/10.1016/j.immuni.2015.02.009

SUMMARY

CD8$^+$ T cells play a critical role in limiting peripheral virus replication, yet how they locate virus-infected cells within tissues is unknown. Here, we have examined the environmental signals that CD8$^+$ T cells use to localize and eliminate virus-infected skin cells. Epicutaneous vaccinia virus (VV) infection, mimicking human smallpox vaccination, greatly increased expression of the CXCR3 chemokine receptor ligands CXCL9 and CXCL10 in VV-infected skin. Despite normal T cell numbers in the skin, *Cxcr3*$^{-/-}$ mice exhibited dramatically impaired CD8$^+$-T-cell-dependent virus clearance. Intravital microscopy revealed that *Cxcr3*$^{-/-}$ T cells were markedly deficient in locating, engaging, and killing virus-infected cells. Further, transfer of wild-type CD8$^+$ T cells restored viral clearance in *Cxcr3*$^{-/-}$ animals. These findings demonstrate a function for CXCR3 in enhancing the ability of tissue-localized CD8$^+$ T cells to locate virus-infected cells and thereby exert anti-viral effector functions.

INTRODUCTION

Viral infections of vertebrates typically begin in mucosal surfaces or the skin, where virions can be introduced by insect bites or directly into cuts or abrasions. Locally released virions often infect adjacent cells but can potentially spread distally via the blood or lymphatics. Viral proteins are delivered to draining lymph nodes (DLNs) as free virions or sub-virion forms or by antigen-presenting cells (APCs) that either are infected with the virus or cross-present viral proteins that they have acquired from other cells. Within DLNs, naive CD8$^+$ T cells survey infected or cross-presenting APCs. Cognate T cells become activated, proliferate, and traffic to peripheral infected tissues to resolve virus infection through a variety of effector mechanisms, including lysing infected cells and releasing antiviral cytokines (Gordon et al., 2011; Liu et al., 2010; Mota et al., 2011).

Recent intravital multiphoton microscopy (MPM) studies into the in vivo function of effector CD8$^+$ T cells have focused on priming in the DLNs, providing great insight into the events leading to naive T cell activation (for reviews, see Henrickson and von Andrian, 2007; Hickman et al., 2011a; Mueller and Hickman, 2010). Less is known about how CD8$^+$ T cells exert their anti-viral functions during active primary infections in the tissue. Using a vaccinia virus (VV) mouse ear-infection model, we defined a central role for CD8$^+$ T cells in clearing mobile virus-infected inflammatory monocytes (Hickman et al., 2013). Although adept at eliminating this subset of infected cells, CD8$^+$ T cells only reluctantly entered compact foci of VV-infected keratinocytes. Thus, highly selective interactions coordinate viral clearance in the tissue.

It is currently unclear how antiviral effector CD8$^+$ T cells locate and further select particular infected cells within a complex tissue environ; however, chemokines often shape cellular movement through a number of mechanisms. Ligation of soluble chemokine to the cognate receptor leads to integrin activation essential for the stable adhesion required for transmigration through inflamed vessels (the role of integrins in interstitial migration is more varied) (Friedl and Weigelin, 2008; Lämmermann et al., 2008; Overstreet et al., 2013). Diffusible chemokine gradients induce cellular chemotaxis in vitro, whereas in vivo chemokines can also be bound to extracellular matrix components and displayed on cell surfaces and thereby promote cell-cell interactions (Hsieh et al., 2006; Proudfoot et al., 2003; Rot, 1993). Chemokine deficiencies lead to enhanced susceptibility to many viral infections in both mice and humans, indicating an important role for chemokine-guided migration in the mitigation of virus-induced pathology (Lim and Murphy, 2011). Although chemokines clearly aid in the entry of immune effectors into infected tissue, their role after cellular entry in shaping migration patterns in situ has not been established during viral infection.

Here, we examined the role of chemokines during cytotoxic T lymphocyte "hunting" of virus-infected cells. Because viruses can cleverly manipulate gene expression in infected cells, it is possible that they control chemokine secretion to prevent detection and thus enhance replication and ultimately host transmission. We imaged T cell location, movement, and function in VV-infected skin, defining a role for CXCR3 ligands in CD8$^+$ T cell recognition and killing of virus-infected cells.

RESULTS

Activated T Cells Contact Peripheral Virus-Infected Cells Lacking Cognate Antigen

We previously reported that after epicutaneous recombinant (thymidine kinase [TK]$^-$) VV inoculation, most infected cells in

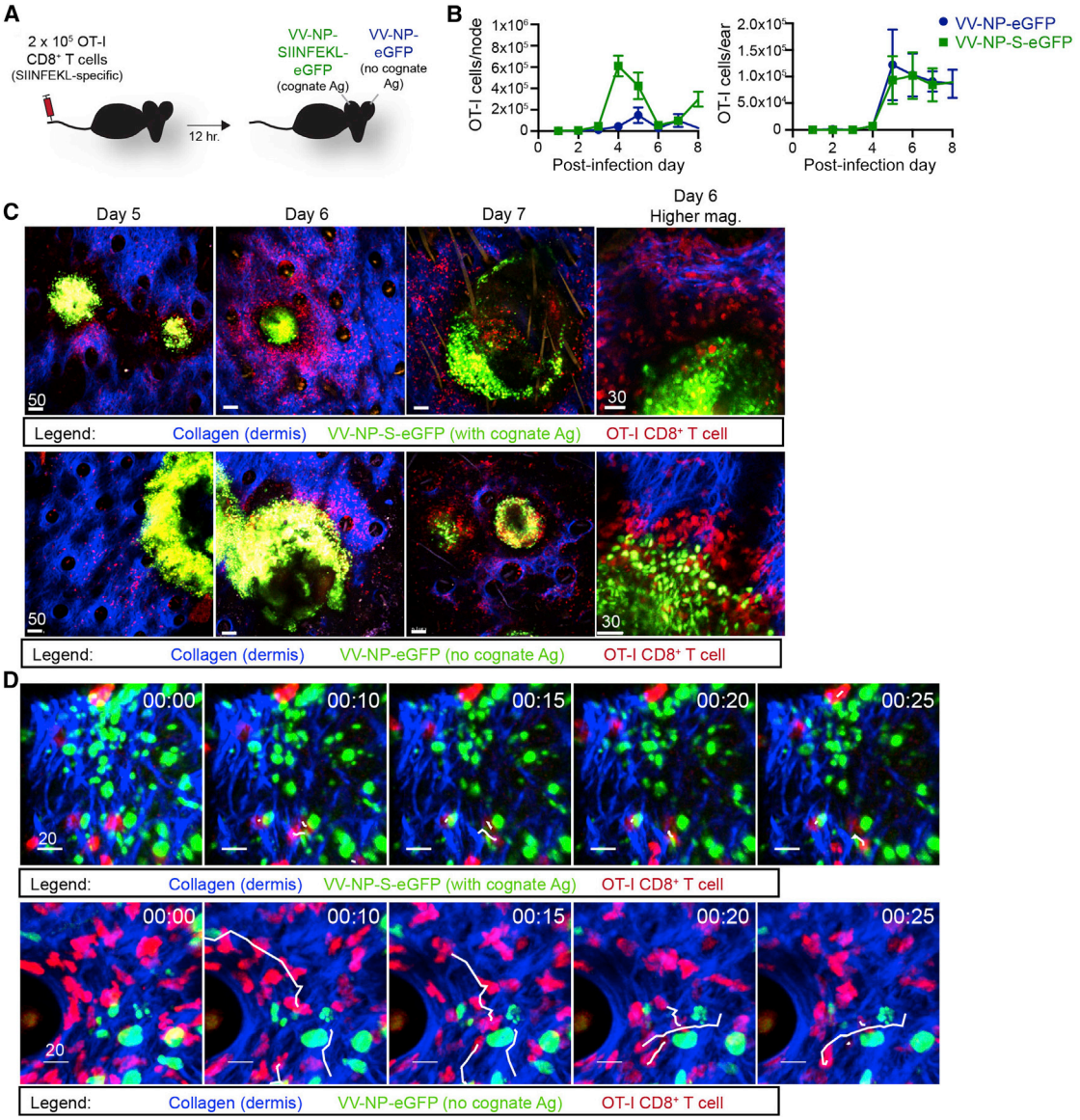

Figure 1. CD8⁺ T Cells Find Virus-Infected Cells that Do Not Express Cognate Ag

(A) Experimental design. A total of 2.5 × 10^5 OT-I T cells were transferred into wild-type (WT) animals prior to epicutaneous infection with VV-NP-S-eGFP (with cognate Ag) in one ear and infection with NP-eGFP (no cognate Ag) in the contralateral ear.

(B) OT-I cells per node (left) or ear (right) as determined by flow cytometric analysis. Infection with NP-S-eGFP (green) and NP-eGFP (blue) is shown. The p.i. day is shown on the x axis. Error bars represent the SEM for n = 3–5 mice per group per time point.

(C) Maximum intensity projections (MIPs) of MPM images of VV-infected ears were taken at the indicated p.i. day (top of images). Dermal collagen (blue), OT-I CD8⁺ T cells (red), and virus-infected cells (green) are shown. Top panels show virus expressing SIINFEKL, and bottom panels show virus lacking SIINFEKL. Higher-magnification images on p.i. day 6 are shown on the far right. Scale bars represent 50 or 30 μm as indicated.

(D) Time-lapse MIP MPM images from p.i. day 5 show contralateral infection as described in (A). White lines indicate paths of selected CD8⁺ T cells during the 25-min imaging period. Scale bars represent 20 μm. Time (upper right-hand corner) is shown in min.

All experiments were repeated three times with n = 3–5 mice/group. See also Figure S1 and Movie S1.

the skin are LY6C⁺ inflammatory monocytes or keratinocytes (Hickman et al., 2013). Activated antigen (Ag)-specific CD8⁺ T cells migrate into the tissue and principally focus on killing infected monocytes rather than keratinocytes (Hickman et al., 2013). To better understand how CD8⁺ T cells locate virus-infected cells, we first examined the contribution of cognate Ag to T cell behavior in VV-infected skin.

Twelve hours after adoptively transferring 2.5 × 10^5 dsRed OT-I T cell receptor (TCR) transgenic CD8⁺ T cells (red, specific for K^b-SIINFEKL) into albino C57BL/6 mice, we inoculated mice epicutaneously with VV-NP-S-eGFP (which expresses SIINFEKL fused to a nuclear-targeted fluorescent protein; Hickman et al., 2011b; Hickman et al., 2008) in one ear and with VV-NP-eGFP (same construct lacking SIINFEKL) in the other ear (Figure 1A).

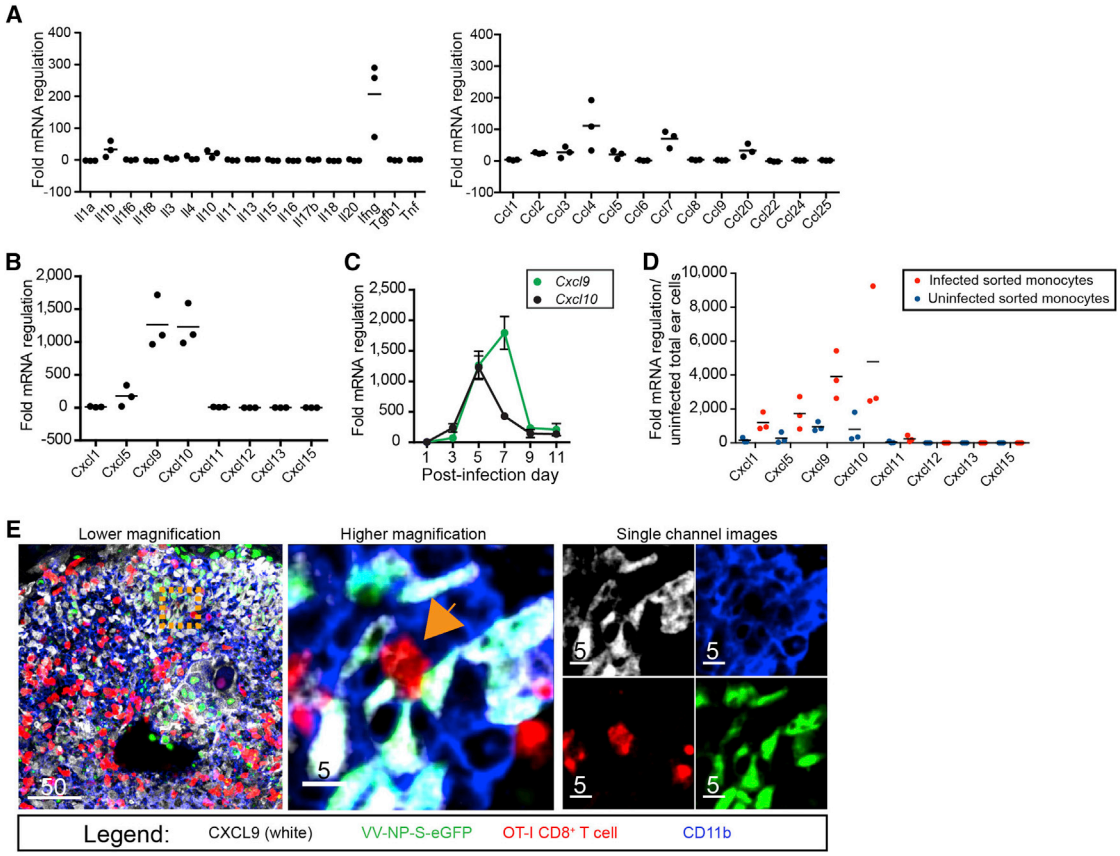

Figure 2. CXCR3 Ligands Are Upregulated in VV-Infected Skin

(A) mRNA regulation in VV-infected ears on p.i. day 5 is compared to that in uninfected ears. Black lines indicate means.

(B) α-chemokine mRNA regulation in VV-infected ears on p.i. day 5 is compared to that in uninfected ears. Black lines indicate means.

(C) *Cxcl9* (green) and *Cxcl10* (blue) mRNA expression in infected skin at the indicated p.i. days (x axis).

(D) mRNA regulation is compared between uninfected (blue dots) and infected (red dots) inflammatory monocytes sorted from day-5 infected ears.

(E) Confocal images taken on p.i. day 5 show frozen tissue sections with VV-NP-S-eGFP (green nuclear staining), CXCL9 (white), OT-I T cells (red), and CD11b (blue). The middle panel shows higher magnification of the orange dashed square from the left panel. The orange arrow indicates an OT-I $CD8^+$ T cell that is interacting with VV-infected $CXCL9^+CD11b^+$ cells. In the right panels, the image from the middle panel is shown with only one color (channel) for clarity. Scale bars represent 50 or 5 μm as indicated.

All experiments were repeated three times. For mRNA data, dots represent separate experiments with n = 2–5 mice/group. See also Figures S2 and S3.

Initially, we enumerated OT-I $CD8^+$ T cells in ears and DLNs at post-infection (p.i.) days 1–8, which spanned the infectious process from the first few infected cells to complete resolution in most cases (Figure 1B; Hickman et al., 2013). OT-I $CD8^+$ T cells increased greatly (~150–600,000) in the lymph node (LN) draining the ear infected with VV-NP-S-eGFP; fewer OT-I cells were recovered from the non-cognate Ag (VV-NP-eGFP) DLN at each time point. Despite the SIINFEKL-dependent disparity in T cell numbers in LNs, cognate Ag had little effect on OT-I T cell numbers in the ear (Figure 1B, right panel). Importantly, OT-I T cells were not recruited to uninfected ears (Figure S1). Thus, VV-induced skin inflammation per se is sufficient to recruit activated T cells in the absence of cognate Ag.

How does cognate Ag affect OT-I $CD8^+$ T cell entry to virus-inflamed skin? MPM imaging of ears on p.i. days 5–7 revealed that Ag was not required for OT-I cells to locate and surround keratinocytic foci of virus replication (Figure 1C) or infected inflammatory monocytes (Figure 1D). Cognate Ag was clearly required, however, for T cells to stably interact with infected monocytes: in the absence of SIINFEKL, OT-I cells quickly scanned infected cells and moved on (shown in white tracks and Movie S1).

Together, these data show that T cells enter VV-infected skin and locate virus-infected cells independently of cognate Ag expression but require Ag to stably interact with infected cells.

Infected Monocytes Produce CXCR3 Ligands in VV-Infected Skin

In order to address which factors govern $CD8^+$ T cell interactions in infected tissue, we performed chemokine- and cytokine-focused qPCR arrays on mRNA isolated from uninfected or infected (p.i. day 5) ear skin (Figure 2). Of 34 cytokine and β-chemokine genes examined, the four greatest increases were in interferon-γ (*Ifng*, upregulated ~200-fold) and β-chemokines genes *Ccl4*, *Ccl7*, and *Ccl20*, whose expression increased ~20- to 100-fold (Figure 2A, right panel). Even greater changes were found in the eight α-chemokine genes tested, two of which,

Cxcl9 and *Cxcl10*, demonstrated >1,000-fold expression increases (Figure 2B). Fine kinetic examination of *Cxcl9* and *Cxcl10* expression revealed parallel increases on day 3 (Figure 2C); *Cxcl10* mRNA peaked on day 5 (concurrent with maximal numbers of infected monocytes; Figure S2), and *Cxcl9* mRNA peaked 2 days later.

We next sorted both infected and uninfected inflammatory monocytes from VV-infected skin (ears) on p.i. day 5 on the basis of VV-encoded GFP expression and cell-surface antibody staining ($CD45^+Ly6C^+CD11b^+$ cells) and analyzed α-chemokine mRNA expression (Figure 2D). Compared to uninfected whole-ear cells (in the absence of infection, the presence of too few monocytes prevents the isolation of a control population), both infected and uninfected inflammatory monocytes displayed increased chemokine mRNA, and infected cells demonstrated much greater (nearly 5,000-fold) increases. The pattern was identical to that seen in the whole ear (the sole exception was that isolated monocytes showed a slight increase in *Cxcl1*, whereas the whole-ear sample did not), consistent with inflammatory monocytes as a principal source of VV-induced chemokines. Note that the increase in infected versus uninfected inflammatory monocytes demonstrates that chemokine mRNA expression was induced by VV infection and is not a general feature of this cell type in situ or an artifact of their isolation from the ear.

To confirm chemokine synthesis, we performed flow cytometric (Figure S3) and microscopic (Figure 2E) analyses of infected ears. Taken at p.i. day 5, confocal images of frozen sections of VV-infected ears showed OT-I $CD8^+$ T cells (red) interacting with VV-infected (green) $CD11b^+$ (blue) cells (inflammatory monocytes). Notably, many infected cells synthesized CXCL9, as indicated by staining in white.

Taken together, our findings indicate that *Cxcl9* and *Cxcl10* mRNAs are highly upregulated in VV-infected skin and that these chemokines are abundantly expressed by infected inflammatory monocytes.

VV Infection Is Exacerbated in *Cxcr3*$^{-/-}$ Mice

To understand the role of CXCL9 and CXCL10 in the recognition of VV-infected cells in vivo, we infected mice deficient in CXCR3, the common receptor for these chemokines (Cole et al., 1998; Mahalingam et al., 1999). On p.i. day 5, we performed confocal imaging to scan large areas of infected skin for hematopoietic cells ($CD45^+$ cells [blue] and virus-infected cells [green]; Figure 3A). As previously described for wild-type (WT) mice, we identified only a small focus of remaining virus-infected cells (Figure 3A, upper middle of left panel). In contrast, *Cxcr3*$^{-/-}$ mice infected in parallel exhibited enormous numbers of virus-infected cells throughout the ear (Figure 3A, right panel). Immunohistochemical staining of ears for CD11b (white) revealed that the majority of infected cells were most likely inflammatory monocytes (Figure 3B).

We next performed flow cytometric analysis of cells from enzymatically dissociated ears to better identify and enumerate infected cell populations (Figure 3C). As previously described (Hickman et al., 2013), at p.i. day 5 WT mice exhibited infiltration of inflammatory monocytes, many of which were infected (GFP^+) (Figure 3C, top panels). Cellular infiltration was remarkably similar in *Cxcr3*$^{-/-}$ mice on p.i. day 5 in that they showed equivalent numbers of inflammatory monocytes (Figures 3C [bottom panels] and 3D). As in WT mice, a majority of infected cells were $LY6CG^{int}$ inflammatory monocytes (Figure 3C [far right panels]). Whereas the total number of inflammatory monocytes was the same at p.i. day 5, the number on day 6 was higher in *Cxcr3*$^{-/-}$ mice. Most importantly, infected inflammatory monocytes were ~4-fold more numerous in *Cxcr3*$^{-/-}$ mice at p.i. day 5 (they peaked at $\sim 7 \times 10^4$ infected monocytes per ear) and remained elevated until p.i. day 8 (Figure 3E). In parallel, *Cxcr3*$^{-/-}$ mice demonstrated increased peak VV titers and most likely delayed complete clearance (Figure 3F).

To determine the cell type responsible for eliminating the virus-infected inflammatory monocytes, we performed antibody-based depletions in WT or *Cxcr3*$^{-/-}$ mice (antibody was given on p.i. days 4 and 5) and then examined ears for the number of infected cells remaining on p.i. day 6 (a time when WT mice have mostly eliminated infected cells under normal conditions) (Figure 3G). As previously reported (Hickman et al., 2013), depletion of $CD8^+$ T cells (but not natural killer [NK] cells) reduced clearance in WT mice (Figure 3G, middle blue bars). $CD8^+$ T cell depletion augmented by 4.5-fold the already higher numbers of inflammatory monocytes in *Cxcr3*$^{-/-}$ mice than in depleted WT mice (green bars).

Together, these data demonstrate that CXCR3 deletion delays $CD8^+$ T cell control of VV-infected inflammatory monocytes, consistent with an important role for CXCL9 and CXCL10 in controlling local VV infection.

VV-Infected *Cxcr3*$^{-/-}$ Mice Exhibit Normal T Cell Activation and Skin Homing

Cxcr3$^{-/-}$ $CD4^+$ OT-II TCR transgenic T cells exhibit defective activation when transferred into WT hosts (Groom et al., 2012). To address whether a similar failure might account for the inability of *Cxcr3*$^{-/-}$ $CD8^+$ T cells to eliminate infected inflammatory monocytes, we generated homozygous *Cxcr3*$^{-/-}$ OT-I TCR transgenic mice and adoptively transferred 2.5×10^5 WT or *Cxcr3*$^{-/-}$ OT-I $CD8^+$ T cells into WT recipients. Two days after infection with SIINFEKL-expressing VV, we removed DLNs and restimulated liberated cells with synthetic SIINFEKL (Figures 4A and 4B). Whereas restimulation with irrelevant peptide yielded background IFN-γ production, both *Cxcr3*$^{-/-}$ and WT cells produced high and equivalent amounts of IFN-γ in response to SIINFEKL restimulation (on the basis of mean fluorescent intensity of positive cells; Figure 4B). Similarly, CXCR3 deficiency did not affect OT-I cells' synthesis of granzyme B (Figure 4C). Accordingly, *Cxcr3*$^{-/-}$ OT-I $CD8^+$ OT-I cells properly homed to the LN peripheral interfollicular regions (Figure 4D), the area in which direct priming occurs in the LN after VV infection (Hickman et al., 2008). Together, these data show that CXCR3 is not required for SIINFEKL-expressing VV-induced activation of OT-I $CD8^+$ T cells in vivo.

CXCR3 can control T cell homing during both infection and autoimmunity (reviewed in Groom and Luster, 2011a, 2011b). Comparing ear-immigrant T cells between WT and *Cxcr3*$^{-/-}$ mice revealed non-statistically significant changes in T cell recruitment (as a percentage of total cellular recruitment) on p.i. days 6 and 7 (Figures 4E and 4F). Ear-derived polyclonal *Cxcr3*$^{-/-}$ $CD8^+$ T cells synthesized IFN-γ in response to restimulation with VV-infected cells or VV-derived peptides (Figure 4F)

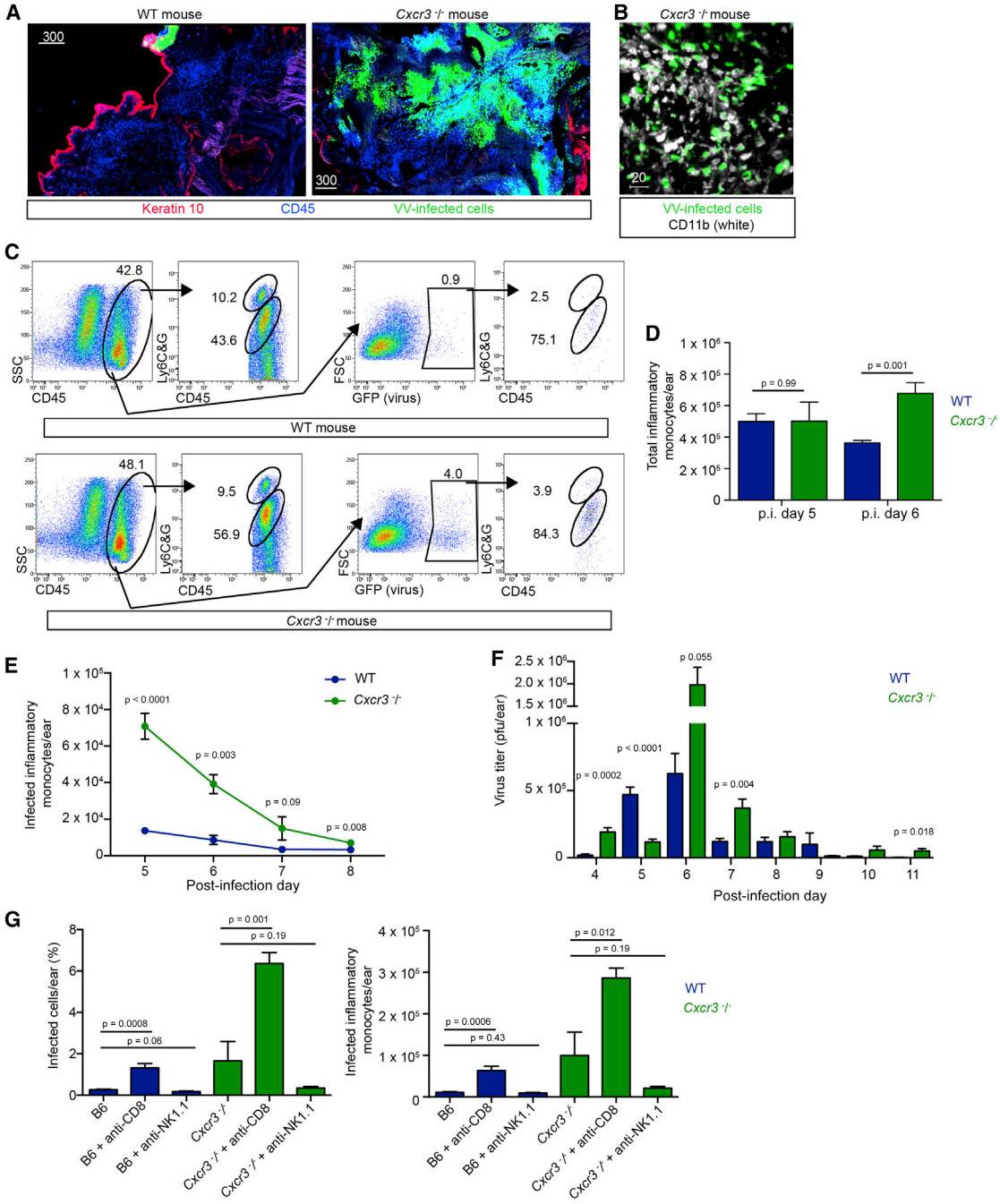

Figure 3. *Cxcr3*$^{-/-}$ Mice Have Elevated Numbers of VV-Infected Inflammatory Monocytes

(A) Confocal montages of frozen sections of WT (left) or *Cxcr3*$^{-/-}$ ears on p.i. day 5 (right). VV-infected cells (green), keratin 10 (red), and CD45 (blue) are shown. Scale bars represent 300 μm.

(B) Confocal image of a *Cxcr3*$^{-/-}$ ear on p.i. day 5. CD11b (white) and VV-infected cells (green) are shown. The scale bar represents 20 μm.

(C) Flow histograms from a dissociated ear on p.i. day 5. Top panels show a WT mouse. Bottom panels show a *Cxcr3*$^{-/-}$ mouse. The second column of dot plots (both WT and *Cxcr3*$^{-/-}$ mice) are gated on total cells. The third column of dot plots show infected (GFP^{+}) cells. The fourth column of dot plots are gated on infected cells and show the percentage of infected cells that are inflammatory monocytes (Ly6CG^{int} cells) and neutrophils (Ly6CG^{hi} cells).

(D) Total inflammatory monocytes on p.i. days 5 and 6 in WT (blue) or *Cxcr3*$^{-/-}$ (green) ears.

(E) Time course of infected inflammatory monocytes in WT (blue) or *Cxcr3*$^{-/-}$ (green) ears.

(F) Titer of infectious virus recovered per ear on the indicated p.i. day in WT (blue) or *Cxcr3*$^{-/-}$ (green) mice.

(G) Percentage and number of infected inflammatory monocytes in WT (blue) or *Cxcr3*$^{-/-}$ (green) ears on p.i. day 6. Ab treatment groups (treatment was performed prior to T cell entrance into the ear on p.i. days 4 and 5) are shown on the x axis.

Error bars represent the SEM. Statistics were obtained by unpaired t tests. All experiments were repeated at least three times with n = 2–5 mice/group.

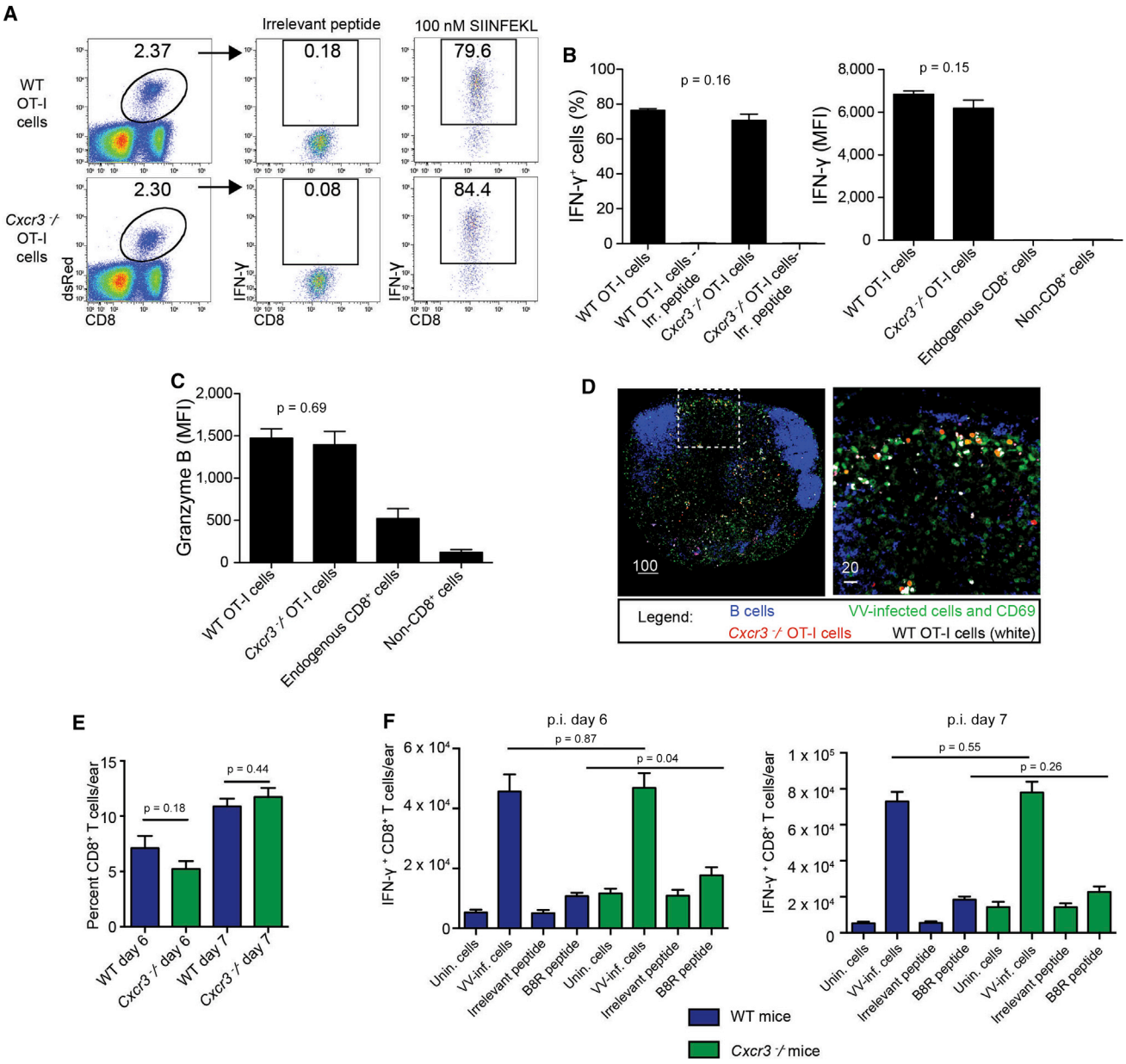

Figure 4. *Cxcr3*$^{-/-}$ CD8$^+$ T Cells Activate and Home Normally

(A) Dot plots from LN cells 2 days after infection with VV-NP-S-eGFP. Mice were given 2.5 × 10^5 WT or *Cxcr3*$^{-/-}$ OT-I CD8$^+$ T cells prior to infection. Gates show the percentage of IFN-γ$^+$ cells after restimulation with the indicated peptide (top).

(B) Percentage (left) and mean fluorescent intensity (MFI, right) of IFN-γ$^+$ cells after restimulation. Endogenous CD8$^+$ cells (all non-transferred CD8$^+$ T cells in the LN) are shown for comparison.

(C) MFI of granzyme B.

(D) Frozen LN sections with VV-infected cells (green), B cells (blue), WT OT-I CD8$^+$ T cells (white), or *Cxcr3*$^{-/-}$ OT-I CD8$^+$ T cells (red) were obtained 8 hr after infection. CD69 is also stained green to indicate activated cells. Scale bars represent 100 (left) or 20 (right) μm.

(E) Percentage of endogenous CD8$^+$ T cells per ear on p.i. days 6 and 7. Blue bars indicate WT cells, and green lines show *Cxcr3*$^{-/-}$ cells.

(F) Number of IFN-γ$^+$ cells per ear in WT (blue) or *Cxcr3*$^{-/-}$ (green) mice on p.i. day 6 (left) or 7 (right).

Error bars represent the SEM. Statistics were obtained by unpaired t tests. All experiments were repeated at least three times with n = 4–6 mice/group.

such that numbers of IFN-γ$^+$CD8$^+$ T cells were similar on p.i. days 6 and 7. *Cxcr3*$^{-/-}$ T cell responses were actually enhanced on p.i. day 6 for B8R (the immunodominant VV determinant in C57BL/6 mice; Tscharke et al., 2005).

On the basis of these findings, we conclude that *Cxcr3*$^{-/-}$ CD8$^+$ T cells exhibit normal activation, tissue homing, and effector cytokine secretion in response to peripheral VV infection.

Cxcr3$^{-/-}$ CD8$^+$ T Cells Fail to Efficiently Engage and Remain in Contact with Virus-Infected Cells in the Tissue

We next assessed the contribution of CXCR3 to CD8$^+$ T cell localization and killing of virus-infected cells. Prior to infection, we co-transferred WT (cyan) and *Cxcr3*$^{-/-}$ (red) OT-I CD8$^+$ T cells into WT mice. On p.i. day 5, we imaged ears infected with VV-NP-S-eGFP (green; Figure 5). Via MPM, we clearly visualized *Cxcr3*$^{-/-}$ CD8$^+$ T cells in the dermis (distinguished by the presence of dermal collagen; Movie S2), consistent with ex vivo flow cytometric analyses showing *Cxcr3*$^{-/-}$ T cell entry into the ear. Like WT cells, *Cxcr3*$^{-/-}$ OT-I CD8$^+$ T cells facilely migrated to surround large, VV-infected keratinocytic foci (Figure 5A; Movie S3).

Given that CD8$^+$ T cell killing of VV-infected inflammatory monocytes contributes to poxvirus clearance in the skin (Hickman et al., 2013), we next assessed the ability of WT (cyan) or *Cxcr3*$^{-/-}$ (red) OT-I cells to locate infected cells (Figure 5B). Both cells located VV-infected cells (previously identified as inflammatory monocytes; Hickman et al., 2013) outlying major keratinocytic lesions (Movie S4). Indeed, we occasionally visualized *Cxcr3*$^{-/-}$ T cells actively pursuing virus-infected cells (Movie S5). Overall, however, whereas high numbers of WT T cells entered fields of virus-infected cells, *Cxcr3*$^{-/-}$ T cells hesitated at the perimeter of heavily infected areas of the tissue (Figure 5C; Movie S6). To quantitate this phenomenon, we acquired (while blinded to the presence of WT cells) MPM images of dense areas of infected monocytes and quantified the percentage (as a function of total cells in the entire field) of WT or *Cxcr3*$^{-/-}$ OT-I cells that had entered areas of infection (Figure 5D). Although WT and *Cxcr3*$^{-/-}$ T cells were equally distributed outside of infected areas of the dermis, a higher percentage of WT T cells than of *Cxcr3*$^{-/-}$ T cells penetrated virus-infected areas (Figure 5D).

We next used MPM to simultaneously track WT (cyan) and *Cxcr3*$^{-/-}$ (red) OT-I CD8$^+$ T cells on p.i. day 5 (Figures 5E–5H). Over 30-min imaging sessions, *Cxcr3*$^{-/-}$ OT-I CD8$^+$ T cells clearly moved faster than WT cells (Figures 5E and 5F; Movie S7). Overlaid tracks of individual cells acquired in the same field of infected cells likewise revealed greater movement of *Cxcr3*$^{-/-}$ T cells (Figure 5E, left panel) than of WT cells (right panel), a feature reflected in average cell speeds over the course of multiple imaging experiments (Figure 5F). On average, WT T cells were >0.5 μm/min slower than *Cxcr3*$^{-/-}$ T cells (Figure 5F, left and middle panels). Similar to *Cxcr3*$^{-/-}$ CD4$^+$ T cells interacting with Ag-pulsed APCs in the LN (Groom et al., 2012), a significantly higher proportion of *Cxcr3*$^{-/-}$ CD8$^+$ T cells present in areas of intense VV infection were highly motile (25.9% versus 16.4%; Figure 5F, right panel).

To determine whether differences in contact with infected cells could account for motility differences, we imaged WT and *Cxcr3*$^{-/-}$ OT-I cells interacting with virus-infected cells in the same field on p.i. day 5; we carefully selected a time period that was late enough for some *Cxcr3*$^{-/-}$ T cells to penetrate infected areas yet not so late that all of the infected cells had been lysed. Whereas many WT OT-I cells contacted infected cells and maintained contact over 30- to 60-min imaging periods, *Cxcr3*$^{-/-}$ OT-I cells were typically more mobile such that they moved from one infected cell to another (Figure 5G; Movie S7). To quantify this, we calculated the percentage of time that a T cell contacted an infected cell during a 1-hr imaging period (note: we did not include any cells that did not stably contact an infected cell within the first 15 min of imaging; Figure 5H). WT T cells remained engaged with virus-infected cells for a longer period after initiating contact (89.3% ± 2.9% [WT] versus 61.2% ± 4.2% [*Cxcr3*$^{-/-}$] of the imaging period). Likewise, although both T cell types rapidly scanned virus-infected cells with which they were engaged, the difference in contact times was reflected in longer pauses (e.g., the cell's time with an instantaneous velocity < 1 μm/min) for WT T cells (63.9% ± 3.5% [WT] versus 36.6% ± 3% [*Cxcr3*$^{-/-}$]; Figure 5H; Figure S4).

Taken together, these data show that relative to WT cells, *Cxcr3*$^{-/-}$ CD8$^+$ T cells exhibit decreased presence in virus-infected regions and shorter contacts with infected cells.

Cxcr3$^{-/-}$ CD8$^+$ T Cells Eliminate Virus-Infected Cells Less Efficiently

To assess the antiviral function of *Cxcr3*$^{-/-}$ versus WT OT-I CD8$^+$ T cells, we transferred 2.5 × 10^5 of either cell type into WT mice, infected them with VV, and analyzed cells for the production of IFN-γ at p.i. day 5.5 (Figures 6A–6D). Although the number of transferred T cells in tissues was similar in both cases (demonstrating the proper homing of activated T cells lacking CXCR3; Figure 6A), direct ex vivo analysis (i.e., without restimulation) revealed that the number of *Cxcr3*$^{-/-}$ OT-I cells producing IFN-γ was lower than that of WT OT-I T cells (Figures 6B and 6C). On a per cell basis, *Cxcr3*$^{-/-}$ and WT OT-I cells synthesized equivalent amounts of IFN-γ, reinforcing the conclusion that CXCR3 expression is not required for CD8$^+$ T cell effector function if the cells have appropriately engaged virus-infected targets (Figure 6D).

We further assessed the ability of *Cxcr3*$^{-/-}$ OT-I cells to control virus infection in vivo by using flow cytometry of cell populations from dissociated ears. We transferred *Cxcr3*$^{-/-}$ or WT OT-I cells into CD8-deficient animals and analyzed their ability to eliminate virus-infected cells (Figure 6E). *Cxcr3*$^{-/-}$ OT-I cells clearly killed fewer infected cells than did WT OT-I cells.

To more systematically examine this phenomenon and precisely control for the number of T cells present in infected tissue, we titrated the number of transferred OT-I cells (ranging from 2.5 × 10^3 to 7.5 × 10^5 per animal) and enumerated both T cells and virus-infected cells in each infected ear (Figures 6F–6J). This enabled us to compare pairs of animals with equivalent numbers of T cells in their ears. For each mouse pair, WT OT-I T cells (blue area) eliminated more infected cells than did *Cxcr3*$^{-/-}$ OT-I cells (green area) (Figure 6F). Over the entire range of adoptively transferred T cells used in Figure 6F, an almost identical number of either WT or *Cxcr3*$^{-/-}$ OT-I cells was present per ear (Figure 6G). Averaging the paired data revealed that WT cells were 4-fold more efficient at eliminating virus-infected cells (Figures 6H and 6I). Finally, WT OT-I cells significantly reduced viral titers when present in numbers equivocal to those of *Cxcr3*$^{-/-}$ T cells (Figure 6J).

These data strongly indicate that *Cxcr3*$^{-/-}$ OT-I cells have a compromised ability to eliminate VV-infected cells.

WT CD8$^+$ T Cells Control Enhanced VV Infection of *Cxcr3*$^{-/-}$ Mice

Although our findings clearly point to an important function for CXCR3 on T cells during the clearance of virus-infected

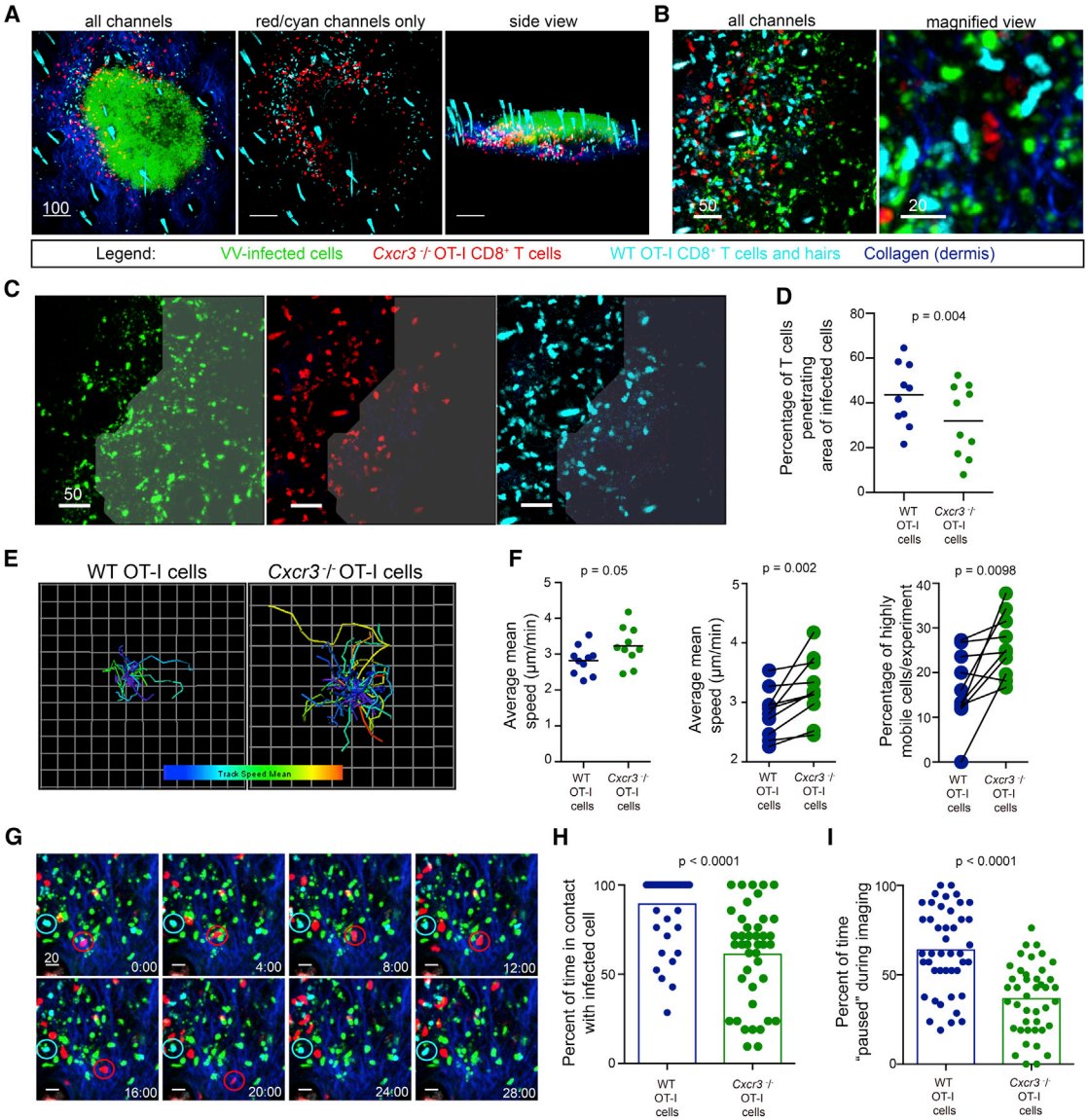

Figure 5. *Cxcr3*$^{-/-}$ CD8^{+} T Cells Have Reduced Entry into Areas of Infection and Decrease Contact with Virus-Infected Cells

(A) MPM images of skin with VV-infected cells (green), dermis (blue), and WT (cyan) or *Cxcr3*$^{-/-}$ (red) OT-I CD8^{+} T cells were taken on p.i. day 5. Note that autofluorescent hairs also appear cyan. Scale bars represent 100 μm.

(B) MPM images from an area with many infected inflammatory monocytes (green). Scale bars represent 50 (left) or 20 (right) μm.

(C) MPM images showing distribution of WT (cyan) or *Cxcr3*$^{-/-}$ (red) OT-I CD8^{+} T cells within a densely infected area (indicated by shading). For clarity, each color is shown independently. Scale bars represent 50 μm.

(D) Percentage of WT (blue) or *Cxcr3*$^{-/-}$ (green) OT-I CD8^{+} T cells within densely infected areas. Dots represent individual microscopic fields. Line represents the mean.

(E) Overlaid tracks of T cells from the same field during a 30-min imaging period. Tracks are color coded from slow (blue) to fast (red).

(F) The left panel shows average mean speeds of WT (blue) or *Cxcr3*$^{-/-}$ (green) OT-I CD8^{+} T cells from the same field in an imaging session (statistics from Mann Whitney test). In the middle panel, WT or *Cxcr3*$^{-/-}$ OT-I T cells in the same field are connected with a line (statistics from Wilcoxon test). The right panel shows the percentage of cells moving >2 SDs from the mean speed of WT OT-I CD8^{+} T cells; lines indicate pairs in the same imaging field (statistics from Wilcoxon test).

(G) Still-frame MPM images of WT (cyan) or *Cxcr3*$^{-/-}$ (red) OT-I T cells over 30 min. A WT cell (cyan circle) and a *Cxcr3*$^{-/-}$ cell (red circle) are followed over time. Scale bars represent 20 μm.

(H) The left panel shows the percentage of time during which WT (blue) and *Cxcr3*$^{-/-}$ (green) cells are contacting infected cells during a 1-hr imaging period. The right panel shows the percentage of time during which WT and *Cxcr3*$^{-/-}$ cells paused on infected cells. Results were combined from two individual experiments and repeated twice.

Time is shown in min. Error bars represent the SEM. All experiments except those in (H) were repeated at least three times with n = 4–6 mice/group. See also Figure S4 and Movies S2, S3, S4, S5, S6, and S7.

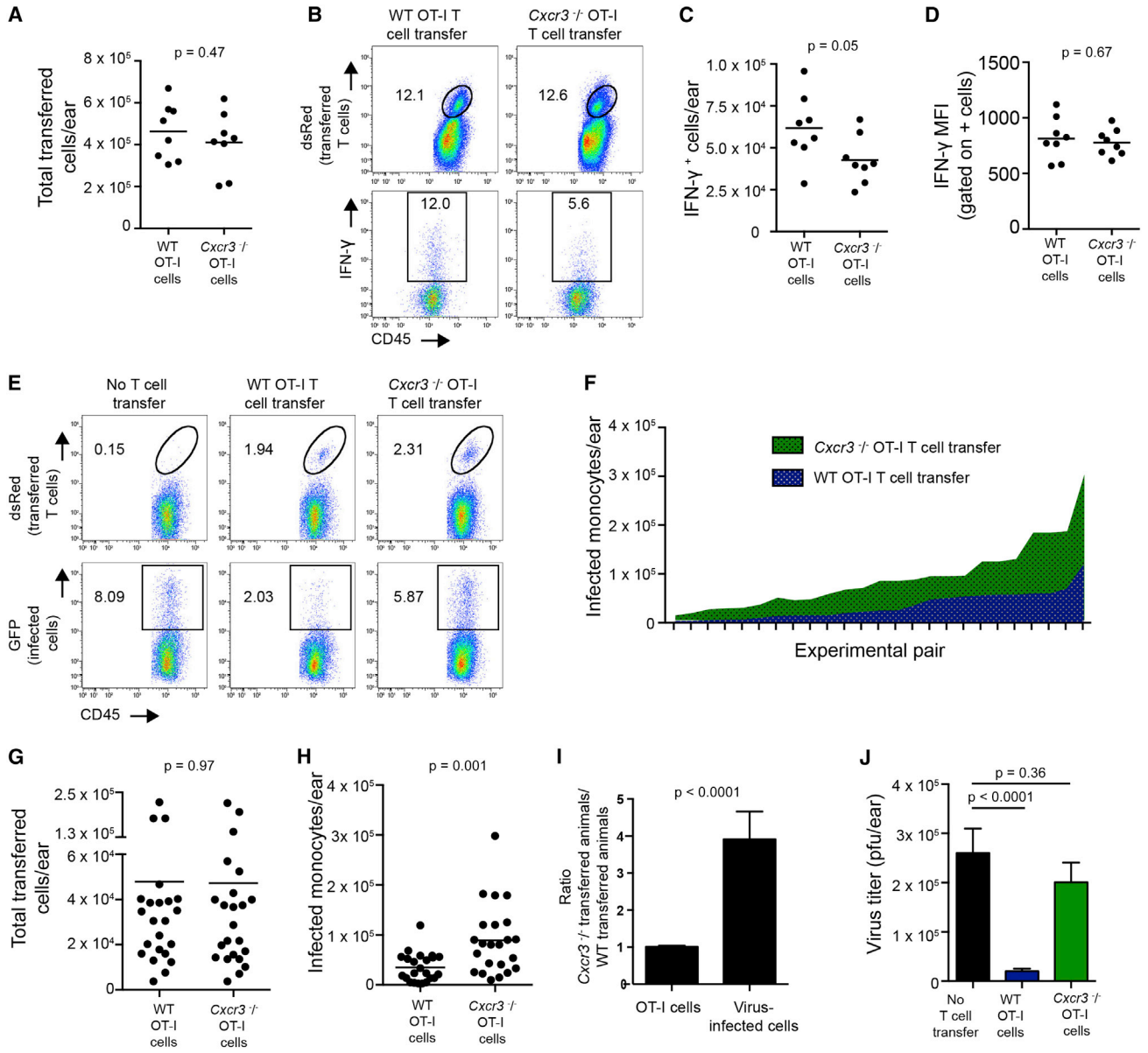

Figure 6. *Cxcr3*$^{-/-}$ CD8$^+$ T Cells Do Not Kill Infected Cells as Efficiently as WT CD8$^+$ T Cells Do

(A) Number of WT or *Cxcr3*$^{-/-}$ OT-I CD8$^+$ T cells on p.i. day 5 after adoptive transfer into WT animals. Dots represent individual ears.

(B) Dot plots gated on the percentage of transferred T cells (dsRed$^+$, top panels) or on IFN-γ$^+$ T cells (bottom panels). WT OT-I cells are on the left, and *Cxcr3*$^{-/-}$ OT-I cells are on the right.

(C) Number of IFN-γ$^+$ cells per ear on p.i. day 5.

(D) MFI of IFN-γ signal from the IFN-γ$^+$ population of transferred cells.

(E) Percentage of transferred cells (top panels) recovered in *Cd8*$^{-/-}$ ears after transfer of 2.5 × 10^5 OT-I cells. No transfer (left panels), WT OT-I cell transfer (middle panels), and *Cxcr3*$^{-/-}$ OT-I transfer (right panels) are shown.

(F) Number of infected cells in *Cd8*$^{-/-}$ ears and titrated numbers (from 2.5 × 10^3 to 7.5 × 10^5) of transferred WT (blue) or *Cxcr3*$^{-/-}$ T (green) cells. The x axis shows pairs of *Cd8*$^{-/-}$ mice in which equivalent numbers of transferred OT-I T cells were recovered.

(G) Number of T cells recovered in *Cd8*$^{-/-}$ mice in the experiment shown in (F).

(H) Number of infected monocytes per ear from the experiment in (F).

(I) Ratios from mice in (F). The left bar shows the number of recovered transferred *Cxcr3*$^{-/-}$ OT-I cells divided by the number of recovered WT OT-I cells. The right bar shows the number of infected cells recovered in animals receiving *Cxcr3*$^{-/-}$ OT-I cells divided by the number of infected cells recovered in animals receiving WT OT-I cells.

(J) Virus titer per ear from the experiment in (F).

Statistics were obtained by a two-tailed Student's unpaired t test (A–C) or a two-tailed paired t test (F). Error bars represent the SEM. Experiments were performed three times with n = 3–4 mice/group (A–C) or five times with n = 2–3 mice/group (F and G).

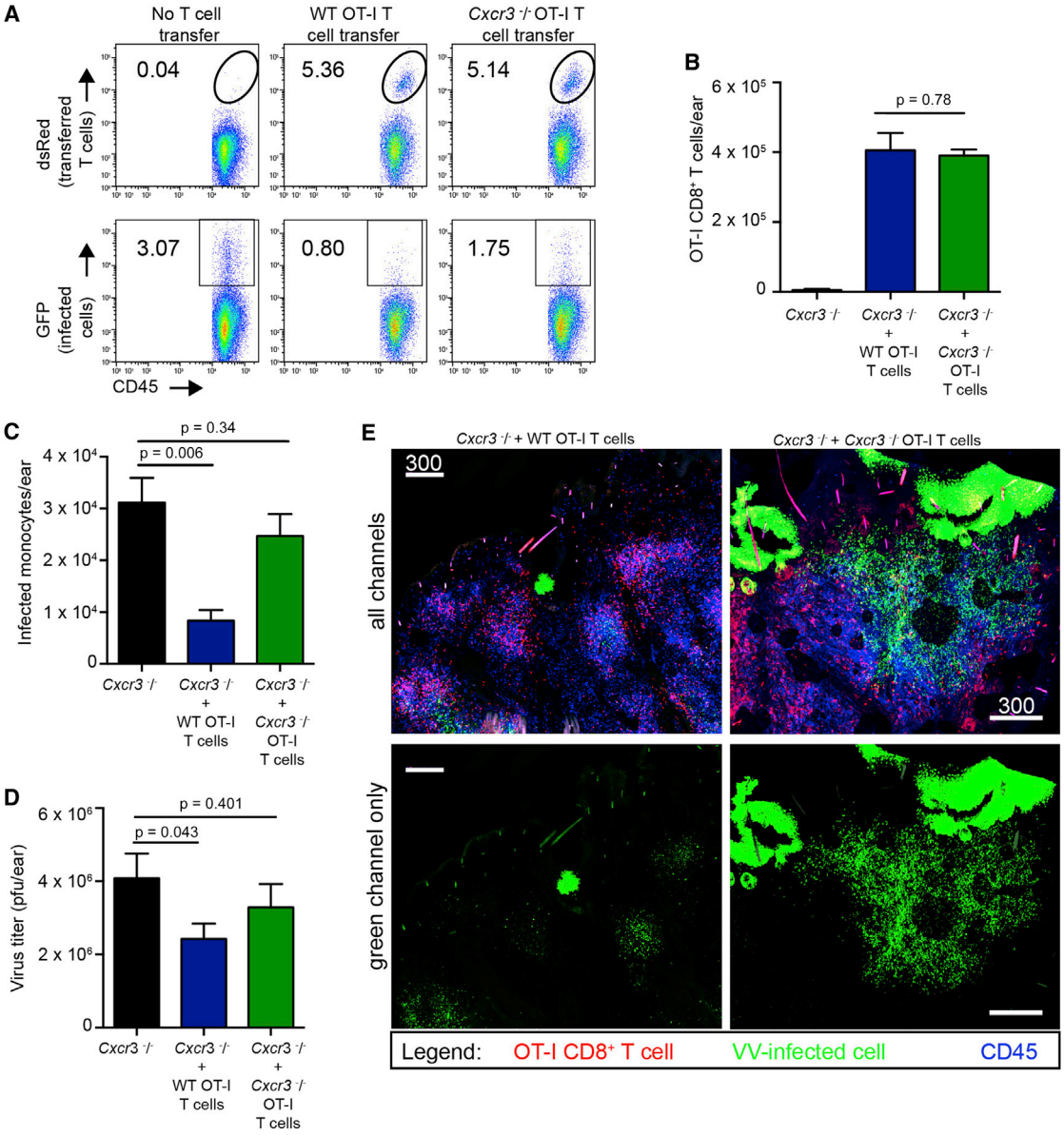

Figure 7. Transfer of WT OT-I CD8$^+$ T Cells into *Cxcr3*$^{-/-}$ Animals Restores Viral Control

(A) Dot plots from *Cxcr3*$^{-/-}$ mice with no T cell transfer (left) or with 2.5 × 10^5 WT (middle) or *Cxcr3*$^{-/-}$ (right) OT-I T cells on p.i. day 5.

(B) Number of adoptively transferred WT or *Cxcr3*$^{-/-}$ OT-I CD8$^+$ T cells recovered per ear in *Cxcr3*$^{-/-}$ animals on p.i. day 5.

(C) Number of virus-infected cells per ear in *Cxcr3*$^{-/-}$ animals adoptively transferred with WT or *Cxcr3*$^{-/-}$ OT-I CD8$^+$ T cells.

(D) Viral titers from (A).

(E) Confocal montage images of *Cxcr3*$^{-/-}$ ears 5 days after infection with VV (green). Mice were transferred with either WT (left) or *Cxcr3*$^{-/-}$ (right) OT-I T cells (red) before infection. CD45$^+$ cells are shown in blue. For clarity, only the green channel is shown in the bottom panels. Scale bars represent 300 μm.

Statistics were obtained by an unpaired two-tailed t test. Error bars represent the SEM.

tissues, it is possible that CXCR3 expression on other cells (innate leukocytes, keratinocytes, etc.) contributes to virus clearance under normal conditions. To address this important issue, we transferred WT or *Cxcr3*$^{-/-}$ OT-I cells into *Cxcr3*$^{-/-}$ mice prior to infection with VV-NP-S-GFP and examined infected ears on p.i. day 5. Both WT and *Cxcr3*$^{-/-}$ OT-I cells efficiently homed to infected *Cxcr3*$^{-/-}$ ears (dsRed$^+$ cells; Figures 7A and7B). Despite the fact that WT and *Cxcr3*$^{-/-}$ OT-I cells had nearly equivalent entry, WT OT-I cells had far fewer infected inflammatory monocytes reflected in diminished viral titers (Figures 7C and 7D). Confocal tile-scan imaging of frozen sections of ears confirmed the absence of large numbers of VV-infected inflammatory monocytes in *Cxcr3*$^{-/-}$ mice that received WT T cells (Figure 7E), which now resembled infected tissue in WT mice (see Figure 3A). Conversely, confocal tile scans from *Cxcr3*$^{-/-}$ animals that received *Cxcr3*$^{-/-}$ OT-I cells more closely mirrored *Cxcr3*$^{-/-}$ animals without T cell transfer (see Figure 3A).

On the basis of these data, we conclude that the positive effects of CXCR3 expression on $CD8^+$ T cell anti-viral activity can be largely, if not completely, ascribed to its function on $CD8^+$ T cells themselves.

DISCUSSION

The chemokine receptor CXCR3 and its ligands play important roles in antiviral immunity. Effector $CD8^+$ T cells upregulate CXCR3 (a transcriptional target of *t-bet*) after infection with a variety of viruses (Taqueti et al., 2006). As a G-protein-coupled chemotactic receptor, CXCR3 affects tissue recruitment of antiviral $CD8^+$ T cells (for examples, see Hokeness et al., 2007; Klein et al., 2005; Lee et al., 2005; Slütter et al., 2013). Additionally, CXCR3 signaling can modify antiviral effector $CD8^+$ T cell differentiation, given that the absence of CXCR3 in murine infections with lymphocytic choriomeningitis virus (LCMV), influenza A virus (IAV), or VV results in increased memory $CD8^+$ T cells at the expense of short-lived effector cells (Hu et al., 2011; Kohlmeier et al., 2011; Kurachi et al., 2011). During secondary viral infections, CXCR3 expression by LN memory effector $CD8^+$ T cells is needed for T cell trafficking to infected peripheral tissues (Kastenmüller et al., 2013; Sung et al., 2012). Additionally, CXCR3 expression allows circulating effector T cells to home to inflamed LNs (Guarda et al., 2007). This is no doubt a partial list of the functions of CXCR3 expression on antiviral $CD8^+$ T cells.

The impact of CXCR3 deficiency on viral replication and pathogenesis in mice varies with the virus studied, although here too, much remains to be learned. *Cxcr3* deficiency increases susceptibility to genital herpes simplex virus type 2 (Thapa and Carr, 2009) and intracerebral dengue virus (Ip and Liao, 2010). Interestingly, protection in each of these models is mediated independently of CXCR3-dependent leukocyte recruitment. CXCR3 deficiency does not appear to alter the outcome of mouse infection with either LCMV (Mahalingam et al., 1999) or herpes simplex virus type 1 (Wickham et al., 2005). Lee et al. (2005) reported no effect on morbidity other than delayed viral clearance in $Cxcr3^{-/-}$ mice infected with murine gammaherpesvirus 68; they attributed this to delayed T cell recruitment, although they also observed deficient $Cxcr3^{-/-}$ T cell lysis of target cells. Likewise, we saw no overt changes in morbidity after epicutaneous VV infection; however, *Cxcr3* deficiency interfered with viral clearance at intermediate times of infection (days 5–7). These data strongly imply that in studies limited to mortality or weight loss as a read-out, additional effects of *Cxcr3* deletion in other virus models could be missed.

Here, we report that CXCR3 can affect not only T cell migration into virus-infected or inflamed tissue but also migration within a tissue as T cells locate virus-infected targets for killing. Although this decreased ability of $Cxcr3^{-/-}$ $CD8^+$ T cells to effectively locate and eliminate infected cells clearly contributes to exacerbated VV infection in $Cxcr3^{-/-}$ mice, it is likely that additional factors also enhance infection in these animals. Prior to the entry of primed T cells into the ear, $Cxcr3^{-/-}$ animals exhibit elevated numbers of infected cells, indicating enhanced early virus replication and/or dissemination independent of T cell control. This suggests a possible role for CXCR3 in innate immune control of early VV replication (CXCR3 is expressed on monocytes, plasmacytoid DCs, and NK cells; Koch et al., 2009). Additionally, $Cxcr3^{-/-}$ mice exhibit delayed dermal wound healing in non-infectious models (Yates et al., 2008; Yates et al., 2007), which could potentially contribute to early VV spread. Whatever the case, the enhanced VV infection we found in $Cxcr3^{-/-}$ mice was controlled by $CD8^+$ T cells, and VV was cleared even in the absence of *Cxcr3*, although this was delayed in comparison to clearance in WT mice.

In the current study, we did not determine all of the cell types synthesizing CXCR3 ligand(s) at different times during infection, partly as a result of concern about the sensitivity of immunohistochemical staining for CXCL9 and CXCL10 (Groom and Luster, 2011b). It will be important to better characterize producing cells in future studies. For this purpose, recently described REX3 mice, which fluorescently report *Cxcl9* and *Cxcl10* expression with different fluorophores (Groom et al., 2012), should be quite useful. At present, however, no system is without additional interpretational complications, given that non-chemokine-producing cells can bind and display functional CXCL9 and CXCL10, which would not be indicated by a fluorescent reporter system (Groom and Luster, 2011b). Importantly, CXCL9 and CXCL10 can be induced by different stimuli and therefore expressed by different repertoires of cells, which can then alter their effects on disease (Groom and Luster, 2011a, 2011b). Further complicating matters, the timing of *Cxcl9* and *Cxcl10* mRNA expression is not identical in VV-infected skin, given that *Cxcl9* mRNA peaks approximately 2 days later than *Cxcl10* mRNA. Thus, it is likely that different populations of cells in the skin (perhaps including non-hematopoietic cellular skin components; Huen and Wells, 2012) produce these two CXCR3 ligands, especially at later times in infection.

Despite these unknowns, the dramatic upregulation of *Cxcl9* and *Cxcl10* mRNA in infected inflammatory monocytes, confirmed by in situ immunohistochemical staining of frozen tissue, suggests that these cells are a major source of CXCR3 ligands. VV-infected inflammatory monocytes largely localize in densely packed dermal areas adjacent to foci of virus replication in keratinocytes (Hickman et al., 2013). Whereas anatomically confined infection most likely results from local virus spread in the tissue, the presence of numerous targets in close proximity greatly enhances the ability of T cells to find and clear infection. Interestingly, we did not observe Levy walk behavior as T cells were hunting virus-infected cells (Harris et al., 2012), most likely because of the heavy density of "prey" (rather than sparse distribution) in the skin. Our data further suggest that infected cells produce a localized gradient of CXCR3 ligands that T cells utilize for entrance into areas of infection. Future studies are required to determine the contribution of serial killing by individual cells versus recruitment of greater numbers of T cells to CXCR3-dependent virus clearance. In the latter case, this would most likely increase the importance of chemokine guidance into heavily infected areas of the tissue.

The interactions and functions mediated by CXCR3 in the tissue are clearly diverse and appropriately complex. Despite this, it might yet be possible to manipulate the system for pragmatic applications. Here, we have shown that CXCR3 maximizes VV clearance in peripheral tissues independently of its influence on tissue immigration, which could potentially be exploited during rational vaccine design. Intriguingly, neutralization of interleukin-12 shortly after IAV immunization boosts the number of

CXCR3-expressing memory CD8$^+$ T cells, which then afford superior protection against subsequent IAV challenge (Slütter et al., 2013). Thus, strategies to increase CXCR3-expressing CD8$^+$ T cells are already in place and might be applied during vaccination to enhance viral clearance by maximizing T cell killing.

EXPERIMENTAL PROCEDURES

Mice

Specific pathogen-free C57BL/6, B6(Cg)-Tyrc-2J/J, STOCK Tg(CAG-DsRed*MST)1Nagy/J, *Cd8*$^{-/-}$ (stock no. 2665), and *Cxcr3*$^{-/-}$ (stock no. 5796) mice were obtained from The Jackson Laboratory or from Taconic Farms. STOCK Tg(CAG-DsRed*MST)1Nagy/J mice were crossed to OT-I TCR transgenic mice (NIAID Intramural Research Repository) and bred for homozygosity for the creation of DsRed OT-I mice. DsRed OT-I mice were crossed with *Cxcr3*$^{-/-}$ mice for the generation of homozygous female *Cxcr3*$^{-/-}$ DsRed OT-I mice. OT-I TCR transgenic mice were also crossed with CFP-expressing mice (B6.129(ICR)-Tg(CAG-ECFP)CK6Nagy/J, stock no. 4218, The Jackson Laboratory) for the creation of WT OT-I CFP mice. 6- to 16-week-old female mice were used in all experiments. All mice were housed under specific pathogen-free conditions (including murine norovirus, mouse parvovirus, and mouse hepatitis virus) and maintained on standard rodent chow and water supplied ad libidum. All animal studies were approved by and performed in accordance with the Animal Care and Use Committee of the National Institute of Allergy and Infectious Diseases.

Viruses and Infections

Mice were anesthetized and infected epicutaneously in the ear by five gentle pokes with a bifurcated needle dipped in VV (stock titer ~1 × 10^8 pfu/ml), as previously described (Hickman et al., 2013). VV-NP-S-eGFP contains the CD8$^+$ T cell determinant SIINFEKL, recognized by OT-I CD8$^+$ T cells; VV-NP-eGFP is an identical virus lacking the SIINFEKL determinant. Viruses were constructed as TK$^-$ viruses in which the recombinant insert was expressed by an early-late vaccinia promoter. Fluorescence expression is an indication of infection rather than the amount of released infectious virions.

T Cell Transfers

CD8$^+$ T cells were purified by negative selection with the use of AutoMACS (Miltenyi Biotec). Cells were 90%–95% pure by flow cytometry. A total of 2.5 × 10^5 (unless dose is otherwise indicated) OT-I cells were transferred intravenously prior to infection. For some multiphoton imaging experiments, WT CFP-expressing OT-I cells and *Cxcr3*$^{-/-}$ dsRed-expressing OT-I cells were co-injected.

Flow Cytometric Analyses

Single-cell suspensions of ears were prepared by collagenase digestion (type I, Worthington Biochemicals) for 1 hr at 37°C prior to filtration through 70-μm nylon cell strainers. Cells were stained with the following antibodies: CD45 (clone 30-F11), CD8 (clone 53-6.7), CD11b (clone M1/70), and Ly6CG (clone Gr-1) (eBioscience). OT-I cells were identified on the basis of CFP or dsRed expression. For intracellular staining for IFN-γ production, brefeldin A (10 μg/ml, Sigma-Aldrich) was added during collagenase digestion, and cells were incubated 2 hr in RPMI containing BFA. Cells were stained, fixed for 20 min with 1% paraformaldehyde, washed, and then stained with anti-IFN-γ (clone XMG1.2) in 0.5% saponin overnight at 4°C. Cells were analyzed on an LSR II flow cytometer (BD Biosciences), and data were analyzed with FlowJo (Tree Star).

Viral Titering via Plaque Assay

Ears were removed at various p.i. times, and collagenase was digested for 1 hr at 37°C and disrupted by vigorous pipetting. This suspension was frozen and thawed three times, sonicated three times, serially diluted, and plated on TK$^-$ cells. Cells were incubated for 2 days before plaques were counted.

Ab Depletion

For Ab-based depletions, 0.5 mg of either anti-CD8 Ab (clone 53-6.7) or anti-NK cell Ab (clone NK1.1) was given intraperitoneally daily beginning on p.i. day 4 (just prior to T cell entry into infected skin), as described in Hickman et al. (2013). Ears were analyzed on p.i. days 5 and 6.

qPCR Arrays

Ears were removed, and the dorsal and ventral halves were separated and immediately deposited in Trizol (Sigma). Ears were chopped into small pieces and then homogenized and passed through a 20-gauge needle. RNA was isolated according to the manufacturer's instructions and then purified with the QIAGEN RNAEasy Mini Kit. On-column DNase digestion was performed prior to RNA elution. cDNAs were made with the RT^2 First Strand Kit (QIAGEN), which started with 2.5 μg of RNA per sample. cDNAs were loaded onto the Inflammatory Cytokines and Receptors qPCR array (PAMM-011Z, QIAGEN), and RT-PCR data were acquired on a RealPlex RT-PCR machine (Eppendorf). Rox was used as a loading control. Expression changes of genes of interest were calculated against five standard housekeeping genes included on the same plate with the use of the manufacturer's data-analysis software based upon ΔΔCT (SABiosciences, now QIAGEN).

Statistics

Statistical significances were calculated by GraphPad (Prism) with the indicated tests. All t tests performed were two tailed.

Confocal Microscopy of Frozen Sections

Ears were removed at the indicated times, fixed overnight in periodate-lysine-paraformaldehyde buffer, and placed in 30% sucrose and PBS for 24 hr before being embedding in optimal-cutting-temperature medium (Electron Microscopy Sciences) and frozen in dry-ice-cooled isopentane. Twenty-micron sections were cut on a Leica cryostat (Leica Microsystems). Sections were blocked with 5% goat, donkey, or rabbit serum and then stained with one or more of the following: CD11b (clone M1/70), B220 (clone RA3-6B2), CD45 (clone 30-F11), CXCL9 (clone MIG-2F5.5, Biolegend), keratin 10 (rabbit polyclonal, Abcam), and/or CD69 (polyclonal goat, R&D Systems).

Intravital MPM Imaging

MPM imaging was performed as described previously (Hickman et al., 2013; Hickman et al., 2008). In brief, images were acquired on an upright Leica SP5 confocal microscope (Leica Microsystems) equipped with two Mai Tai Ti:Sapphire lasers (Spectra Physics). Ears were immobilized and bathed in warm saline. Images were acquired with a 20× dipping objective (numerical aperture = 1.00). Images were obtained at 900 nm for eGFP-collagen-dsRed imaging. Imaging of CFP-collagen-GFP-sRed was performed in sequential mode at 900 and 800 nm (for CFP excitation). Emitted fluorescence was collected with a four-channel non-descanned detector. Wavelength separation was accomplished with a 495-nm dichroic mirror followed by emission filters of 460/50 nm and 525/50 nm. The red channel was collected by a detector after it passed through a 560-nm dichroic with a 610/60 bandpass emission filter. For most movies (e.g., when time was critical), images were acquired with 2× zoom and a 3-μm z step for a total depth of 45 μm every 30 s. During sequential mode, this time interval was extended to 1–3 min between series (to allow for switching lasers).

MPM Analysis

Maximum intensity projections were processed from z stacks with Imaris (Bitplane). For tracking cellular movement, images were processed with a Gaussian filter, and then tracks were calculated with the "spot" function. Overlaid tracks were generated with Imaris XT function "translate tracks" and were pseudocolored according to the average speed of the cell creating the track. Average speeds were calculated with the following parameters: autoregressive motion, gapclose 1, 7.5-μm object diameter, and 20-μm maximum distance. Created tracks were analyzed individually by hand for erroneous connections.

For analysis of the percentage of T cells that entered virus-infected areas, microscopic fields were selected on the basis of the presence of high densities of GFP$^+$ non-keratinocytic infected cells. Fields were collected so that approximately 50%–75% of the field contained infected cells, and this process was blinded to the presence of WT T cells. WT and *Cxcr3*$^{-/-}$ T cells were enumerated with spot-detection software (Imaris) inside and outside the area of infected cells. The percentage of WT or *Cxcr3*$^{-/-}$ CD8$^+$ T cells within the area

of virus-infected cells (as a function of the total number of T cells present in the image) was then calculated. Data were plotted with GraphPad Software (Prism).

For analysis of contact times with infected cells, it was critical to wait until p.i. days 5.5–6.0, when *Cxcr3*$^{-/-}$ T cells had time to enter areas of viral infection (but infected cells had not yet been lysed). One-hour movies were collected with a 4-μm z step at 2× magnification. Tracks were created manually because the large number of cells present resulted in erroneous classifications by automated tracking. Contact time per infected cell was manually assigned for 15–30 cells per independent experiment and reported as a percentage of time in contact during the total 1-hr imaging period. The number of "pause" steps was calculated automatically with the ImarisXT function "calculate track length" with an input pausing value of 1 μm/min.

SUPPLEMENTAL INFORMATION

Supplemental Information includes four figures and seven movies and can be found with this article online at http://dx.doi.org/10.1016/j.immuni.2015.02.009.

ACKNOWLEDGMENTS

The authors would like to thank members of the Comparative Medicine Branch for excellence in animal husbandry, the NIAID flow cytometry facility (Bishop Hague and Elina Stregevsky) for cell sorting, and the NIAID Biological Imaging facility (Owen Schwartz) for assistance with microscopy. This work was supported by the Intramural Research Program of the NIAID, NIH.

Received: August 26, 2014
Revised: January 8, 2015
Accepted: February 20, 2015
Published: March 10, 2015

REFERENCES

Cole, K.E., Strick, C.A., Paradis, T.J., Ogborne, K.T., Loetscher, M., Gladue, R.P., Lin, W., Boyd, J.G., Moser, B., Wood, D.E., et al. (1998). Interferon-inducible T cell alpha chemoattractant (I-TAC): a novel non-ELR CXC chemokine with potent activity on activated T cells through selective high affinity binding to CXCR3. J. Exp. Med. *187*, 2009–2021.

Friedl, P., and Weigelin, B. (2008). Interstitial leukocyte migration and immune function. Nat. Immunol. *9*, 960–969.

Gordon, S.N., Cecchinato, V., Andresen, V., Heraud, J.M., Hryniewicz, A., Parks, R.W., Venzon, D., Chung, H.K., Karpova, T., McNally, J., et al. (2011). Smallpox vaccine safety is dependent on T cells and not B cells. J. Infect. Dis. *203*, 1043–1053.

Groom, J.R., and Luster, A.D. (2011a). CXCR3 in T cell function. Exp. Cell Res. *317*, 620–631.

Groom, J.R., and Luster, A.D. (2011b). CXCR3 ligands: redundant, collaborative and antagonistic functions. Immunol. Cell Biol. *89*, 207–215.

Groom, J.R., Richmond, J., Murooka, T.T., Sorensen, E.W., Sung, J.H., Bankert, K., von Andrian, U.H., Moon, J.J., Mempel, T.R., and Luster, A.D. (2012). CXCR3 chemokine receptor-ligand interactions in the lymph node optimize CD4+ T helper 1 cell differentiation. Immunity *37*, 1091–1103.

Guarda, G., Hons, M., Soriano, S.F., Huang, A.Y., Polley, R., Martín-Fontecha, A., Stein, J.V., Germain, R.N., Lanzavecchia, A., and Sallusto, F. (2007). L-selectin-negative CCR7- effector and memory CD8+ T cells enter reactive lymph nodes and kill dendritic cells. Nat. Immunol. *8*, 743–752.

Harris, T.H., Banigan, E.J., Christian, D.A., Konradt, C., Tait Wojno, E.D., Norose, K., Wilson, E.H., John, B., Weninger, W., Luster, A.D., et al. (2012). Generalized Lévy walks and the role of chemokines in migration of effector CD8+ T cells. Nature *486*, 545–548.

Henrickson, S.E., and von Andrian, U.H. (2007). Single-cell dynamics of T-cell priming. Curr. Opin. Immunol. *19*, 249–258.

Hickman, H.D., Takeda, K., Skon, C.N., Murray, F.R., Hensley, S.E., Loomis, J., Barber, G.N., Bennink, J.R., and Yewdell, J.W. (2008). Direct priming of antiviral CD8+ T cells in the peripheral interfollicular region of lymph nodes. Nat. Immunol. *9*, 155–165.

Hickman, H.D., Bennink, J.R., and Yewdell, J.W. (2011a). From optical bench to cageside: intravital microscopy on the long road to rational vaccine design. Immunol. Rev. *239*, 209–220.

Hickman, H.D., Li, L., Reynoso, G.V., Rubin, E.J., Skon, C.N., Mays, J.W., Gibbs, J., Schwartz, O., Bennink, J.R., and Yewdell, J.W. (2011b). Chemokines control naive CD8+ T cell selection of optimal lymph node antigen presenting cells. J. Exp. Med. *208*, 2511–2524.

Hickman, H.D., Reynoso, G.V., Ngudiankama, B.F., Rubin, E.J., Magadán, J.G., Cush, S.S., Gibbs, J., Molon, B., Bronte, V., Bennink, J.R., and Yewdell, J.W. (2013). Anatomically restricted synergistic antiviral activities of innate and adaptive immune cells in the skin. Cell Host Microbe *13*, 155–168.

Hokeness, K.L., Deweerd, E.S., Munks, M.W., Lewis, C.A., Gladue, R.P., and Salazar-Mather, T.P. (2007). CXCR3-dependent recruitment of antigen-specific T lymphocytes to the liver during murine cytomegalovirus infection. J. Virol. *81*, 1241–1250.

Hsieh, M.F., Lai, S.L., Chen, J.P., Sung, J.M., Lin, Y.L., Wu-Hsieh, B.A., Gerard, C., Luster, A., and Liao, F. (2006). Both CXCR3 and CXCL10/IFN-inducible protein 10 are required for resistance to primary infection by dengue virus. J. Immunol. *177*, 1855–1863.

Hu, J.K., Kagari, T., Clingan, J.M., and Matloubian, M. (2011). Expression of chemokine receptor CXCR3 on T cells affects the balance between effector and memory CD8 T-cell generation. Proc. Natl. Acad. Sci. USA *108*, E118–E127.

Huen, A.C., and Wells, A. (2012). The Beginning of the End: CXCR3 Signaling in Late-Stage Wound Healing. Adv. Wound Care (New Rochelle) *1*, 244–248.

Ip, P.P., and Liao, F. (2010). Resistance to dengue virus infection in mice is potentiated by CXCL10 and is independent of CXCL10-mediated leukocyte recruitment. J. Immunol. *184*, 5705–5714.

Kastenmüller, W., Brandes, M., Wang, Z., Herz, J., Egen, J.G., and Germain, R.N. (2013). Peripheral prepositioning and local CXCL9 chemokine-mediated guidance orchestrate rapid memory CD8+ T cell responses in the lymph node. Immunity *38*, 502–513.

Klein, R.S., Lin, E., Zhang, B., Luster, A.D., Tollett, J., Samuel, M.A., Engle, M., and Diamond, M.S. (2005). Neuronal CXCL10 directs CD8+ T-cell recruitment and control of West Nile virus encephalitis. J. Virol. *79*, 11457–11466.

Koch, M.A., Tucker-Heard, G., Perdue, N.R., Killebrew, J.R., Urdahl, K.B., and Campbell, D.J. (2009). The transcription factor T-bet controls regulatory T cell homeostasis and function during type 1 inflammation. Nat. Immunol. *10*, 595–602.

Kohlmeier, J.E., Reiley, W.W., Perona-Wright, G., Freeman, M.L., Yager, E.J., Connor, L.M., Brincks, E.L., Cookenham, T., Roberts, A.D., Burkum, C.E., et al. (2011). Inflammatory chemokine receptors regulate CD8(+) T cell contraction and memory generation following infection. J. Exp. Med. *208*, 1621–1634.

Kurachi, M., Kurachi, J., Suenaga, F., Tsukui, T., Abe, J., Ueha, S., Tomura, M., Sugihara, K., Takamura, S., Kakimi, K., and Matsushima, K. (2011). Chemokine receptor CXCR3 facilitates CD8(+) T cell differentiation into short-lived effector cells leading to memory degeneration. J. Exp. Med. *208*, 1605–1620.

Lämmermann, T., Bader, B.L., Monkley, S.J., Worbs, T., Wedlich-Söldner, R., Hirsch, K., Keller, M., Förster, R., Critchley, D.R., Fässler, R., and Sixt, M. (2008). Rapid leukocyte migration by integrin-independent flowing and squeezing. Nature *453*, 51–55.

Lee, B.J., Giannoni, F., Lyon, A., Yada, S., Lu, B., Gerard, C., and Sarawar, S.R. (2005). Role of CXCR3 in the immune response to murine gammaherpesvirus 68. J. Virol. *79*, 9351–9355.

Lim, J.K., and Murphy, P.M. (2011). Chemokine control of West Nile virus infection. Exp. Cell Res. *317*, 569–574.

Liu, L., Zhong, Q., Tian, T., Dubin, K., Athale, S.K., and Kupper, T.S. (2010). Epidermal injury and infection during poxvirus immunization is crucial for the generation of highly protective T cell-mediated immunity. Nat. Med. *16*, 224–227.

Mahalingam, S., Farber, J.M., and Karupiah, G. (1999). The interferon-inducible chemokines MuMig and Crg-2 exhibit antiviral activity In vivo. J. Virol. *73*, 1479–1491.

Mota, B.E., Gallardo-Romero, N., Trindade, G., Keckler, M.S., Karem, K., Carroll, D., Campos, M.A., Vieira, L.Q., da Fonseca, F.G., Ferreira, P.C., et al. (2011). Adverse events post smallpox-vaccination: insights from tail scarification infection in mice with Vaccinia virus. PLoS ONE *6*, e18924.

Mueller, S.N., and Hickman, H.D. (2010). In vivo imaging of the T cell response to infection. Curr. Opin. Immunol. *22*, 293–298.

Overstreet, M.G., Gaylo, A., Angermann, B.R., Hughson, A., Hyun, Y.M., Lambert, K., Acharya, M., Billroth-Maclurg, A.C., Rosenberg, A.F., Topham, D.J., et al. (2013). Inflammation-induced interstitial migration of effector $CD4^+$ T cells is dependent on integrin αV. Nat. Immunol. *14*, 949–958.

Proudfoot, A.E., Handel, T.M., Johnson, Z., Lau, E.K., LiWang, P., Clark-Lewis, I., Borlat, F., Wells, T.N., and Kosco-Vilbois, M.H. (2003). Glycosaminoglycan binding and oligomerization are essential for the in vivo activity of certain chemokines. Proc. Natl. Acad. Sci. USA *100*, 1885–1890.

Rot, A. (1993). Neutrophil attractant/activation protein-1 (interleukin-8) induces in vitro neutrophil migration by haptotactic mechanism. Eur. J. Immunol. *23*, 303–306.

Slütter, B., Pewe, L.L., Kaech, S.M., and Harty, J.T. (2013). Lung airway-surveilling CXCR3(hi) memory CD8(+) T cells are critical for protection against influenza A virus. Immunity *39*, 939–948.

Sung, J.H., Zhang, H., Moseman, E.A., Alvarez, D., Iannacone, M., Henrickson, S.E., de la Torre, J.C., Groom, J.R., Luster, A.D., and von Andrian, U.H. (2012). Chemokine guidance of central memory T cells is critical for antiviral recall responses in lymph nodes. Cell *150*, 1249–1263.

Taqueti, V.R., Grabie, N., Colvin, R., Pang, H., Jarolim, P., Luster, A.D., Glimcher, L.H., and Lichtman, A.H. (2006). T-bet controls pathogenicity of CTLs in the heart by separable effects on migration and effector activity. J. Immunol. *177*, 5890–5901.

Thapa, M., and Carr, D.J. (2009). CXCR3 deficiency increases susceptibility to genital herpes simplex virus type 2 infection: Uncoupling of CD8+ T-cell effector function but not migration. J. Virol. *83*, 9486–9501.

Tscharke, D.C., Karupiah, G., Zhou, J., Palmore, T., Irvine, K.R., Haeryfar, S.M., Williams, S., Sidney, J., Sette, A., Bennink, J.R., and Yewdell, J.W. (2005). Identification of poxvirus CD8+ T cell determinants to enable rational design and characterization of smallpox vaccines. J. Exp. Med. *201*, 95–104.

Wickham, S., Lu, B., Ash, J., and Carr, D.J. (2005). Chemokine receptor deficiency is associated with increased chemokine expression in the peripheral and central nervous systems and increased resistance to herpetic encephalitis. J. Neuroimmunol. *162*, 51–59.

Yates, C.C., Whaley, D., Kulasekeran, P., Hancock, W.W., Lu, B., Bodnar, R., Newsome, J., Hebda, P.A., and Wells, A. (2007). Delayed and deficient dermal maturation in mice lacking the CXCR3 ELR-negative CXC chemokine receptor. Am. J. Pathol. *171*, 484–495.

Yates, C.C., Whaley, D., Y-Chen, A., Kulesekaran, P., Hebda, P.A., and Wells, A. (2008). ELR-negative CXC chemokine CXCL11 (IP-9/I-TAC) facilitates dermal and epidermal maturation during wound repair. Am. J. Pathol. *173*, 643–652.